Supplementary Materials for

JAK inhibition enhances checkpoint blockade immunotherapy in patients with Hodgkin lymphoma

Authors: Jaroslav Zak*†, Isaraphorn Pratumchai†, Brett S. Marro†‡, Kristi L. Marquardt, Reza Beheshti Zavareh§, Luke L. Lairson, Michael B. A. Oldstone, Judith A. Varner, Livia Hegerova, Qing Cao, Umar Farooq, Vaishalee P. Kenkre, Veronika Bachanova*¶, John R. Teijaro*¶

† These authors contributed equally

¶Co-senior authors

*Corresponding authors. Email: jaroslav@scripps.edu, bach0173@umn.edu and teijaro@scripps.edu

The PDF file includes:

Figs. S1 to S17
Tables S1 to S3

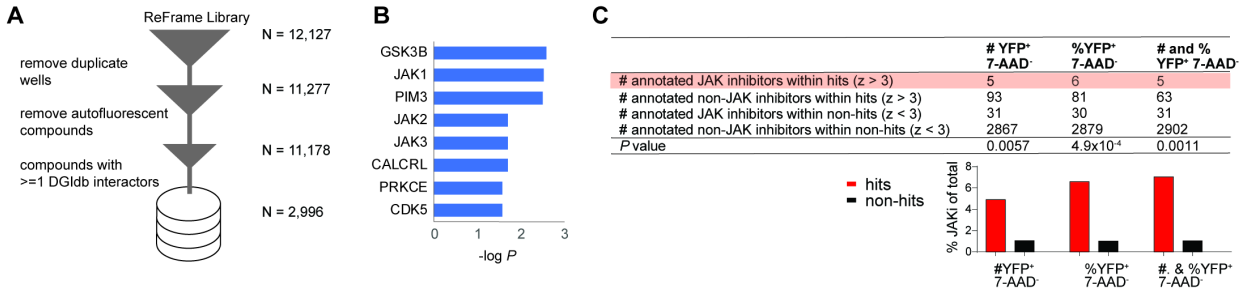

	# YFP+ 7-AAD-	%YFP+ 7-AAD-	# and % YFP+ 7-AAD-
# annotated JAK inhibitors within hits (z > 3)	5	6	5
# annotated non-JAK inhibitors within hits (z > 3)	93	81	63
# annotated JAK inhibitors within non-hits (z < 3)	31	30	31
# annotated non-JAK inhibitors within non-hits (z < 3)	2867	2879	2902
P value	0.0057	4.9×10^{-4}	0.0011

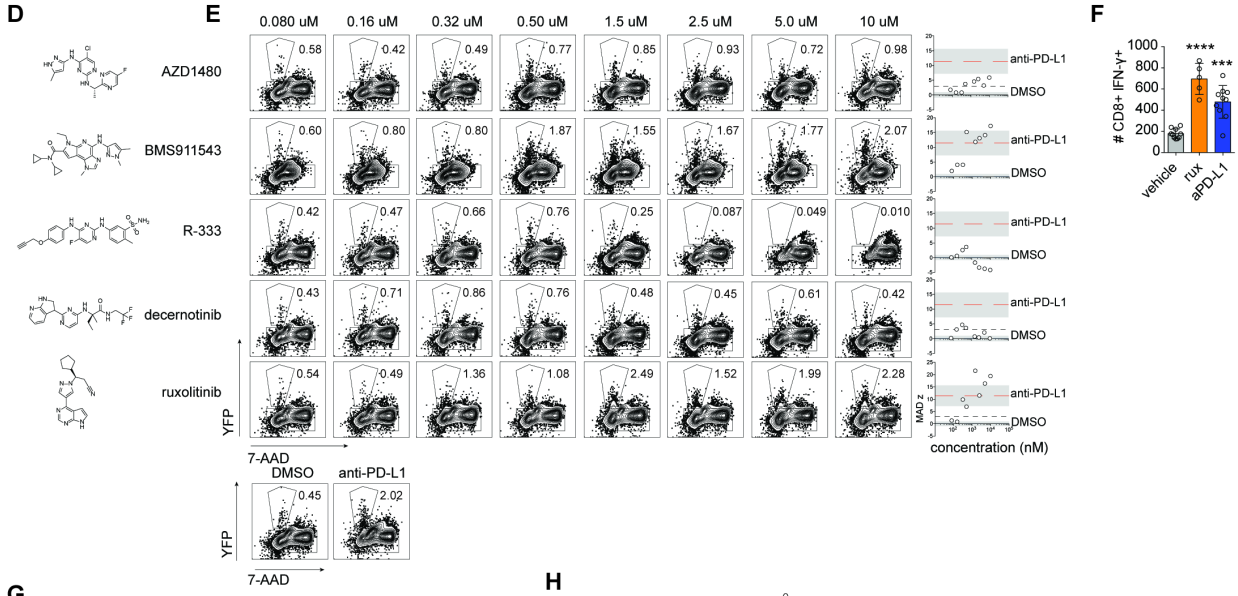

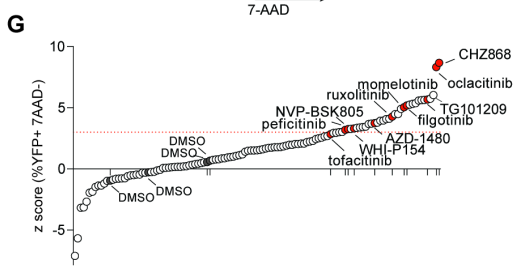

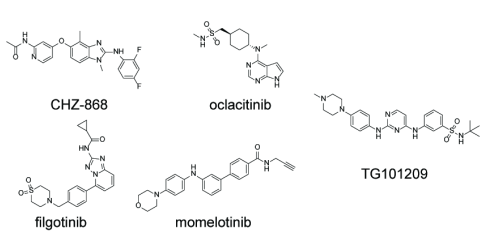

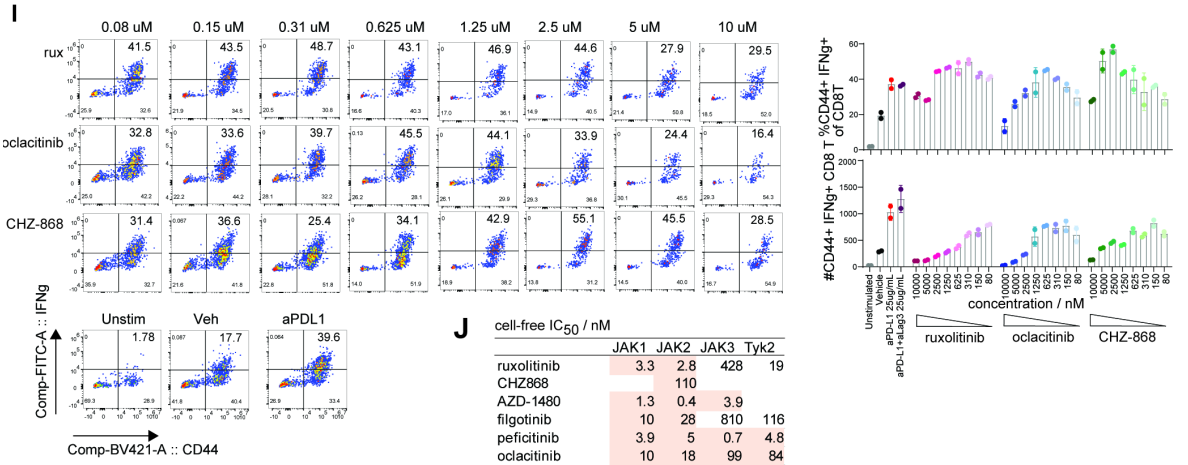

J

cell-free IC_{50} / nM

	JAK1	JAK2	JAK3	Tyk2
ruxolitinib	3.3	2.8	428	19
CHZ868		110		
AZD-1480	1.3	0.4	3.9	
filgotinib	10	28	810	116
peficitinib	3.9	5	0.7	4.8
oclacitinib	10	18	99	84
TG101209		6	169	
NVP-BSK805	31.6	0.48	18.7	10.76
BMS911543	356	1.1	73	66

Supplementary Figure 1. (**A-C, E-H**) Splenocytes from Cl13 infected IFNγ-IRES-YFP mice were harvested at 15 days post infection and cultured in the presence of LCMV peptides for 5 days (more details see Materials and Methods). (A) Preprocessing of ReFrame metadata for drug-target analysis, counts in right column indicate number of compounds at each step. (B) Protein targets most highly enriched in hit vs non-hit compounds, targets were ranked by Fisher test p value and known drug metabolism enzymes were filtered out. (C) Summary of JAK inhibitor enrichment in hit vs non-hit groups using database-annotated compounds as described in panel A. (**D**) Chemical structures of top JAK inhibitor hits in the ReFrame library screen. (E) results of validation assay of re-obtained JAK inhibitor hits performed as the primary screening assay at a range of concentrations for each compound. (F) total number of IFNg+ CD8 T cells measured in panel 1A. (G) Ranking of compounds from kinase inhibitor library by z-score of $\%YFP^+$ $7\text{-}AAD^-$, JAKi marked in red, vehicle (DMSO only) controls highlighted in text. (H) Chemical structures of top 5 hits from kinase inhibitor library (MedChemExpress). (**I**) Results of validation assay equivalent to panel E performed with oclacitinib and CHZ-868. (**J**) Cell-free IC_{50} values from JAK family inhibition assays of top JAKi hits from kinase inhibitor library, for list of references see Materials and methods. Screening experiment was performed once with duplicates (*18*); validation experiments were performed 1-2 for most JAK inhibitors and at least 3 times for ruxolitinib. Statistical comparison of experimental groups was performed using Fisher's exact test (B-C), one-way ANOVA and Dunnett's post-test (F); *, $p \leq 0.05$; **, $p \leq 0.01$; ***, $p \leq 0.001$; ****, $p \leq 0.0001$.

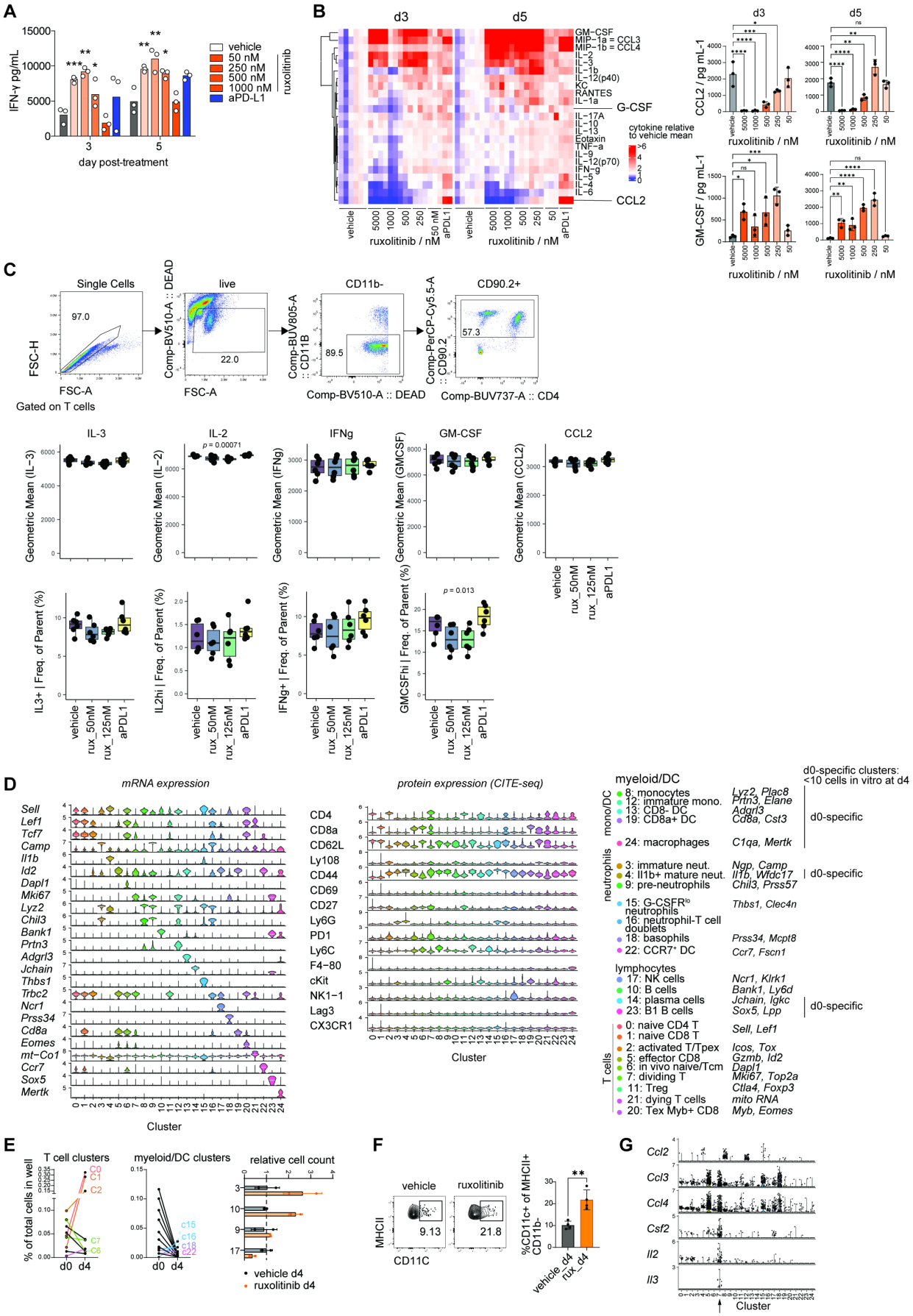
A
IFN-γ pg/mL
day post-treatment
vehicle
50 nM
250 nM
500 nM
1000 nM
aPD-L1
ruxolitinib
B
d3
d5
GM-CSF
MIP-1a = CCL3
MIP-1b = CCL4
IL-2
IL-3
IL-1b
IL-12(p40)
KC
RANTES
IL-1a
G-CSF
IL-17A
IL-10
IL-13
Eotaxin
TNF-a
IL-9
IL-12(p70)
IFN-g
IL-5
IL-4
IL-6
CCL2
cytokine relative to vehicle mean
ruxolitinib / nM
CCL2 / pg mL-1
GM-CSF / pg mL-1
C
Single Cells
live
CD11b-
CD90.2+
FSC-H
FSC-A
Gated on T cells
Comp-BV510-A :: DEAD
Comp-BUV805-A :: CD11B
Comp-PerCP-Cy5.5-A CD90.2 ::
Comp-BUV737-A :: CD4
97.0
22.0
89.5
57.3
IL-3
IL-2
IFNg
GM-CSF
CCL2
Geometric Mean (IL-3)
Geometric Mean (IL-2)
Geometric Mean (IFNg)
Geometric Mean (GMCSF)
Geometric Mean (CCL2)
p = 0.00071
p = 0.013
IL3+ | Freq. of Parent (%)
IL2hi | Freq. of Parent (%)
IFNg+ | Freq. of Parent (%)
GMCSFhi | Freq. of Parent (%)
vehicle
rux_50nM
rux_125nM
aPDL1
D
mRNA expression
protein expression (CITE-seq)
Sell
Lef1
Tcf7
Camp
Il1b
Id2
Dapl1
Mki67
Lyz2
Chil3
Bank1
Prtn3
Adgrl3
Jchain
Thbs1
Trbc2
Ncr1
Prss34
Cd8a
Eomes
mt-Co1
Ccr7
Sox5
Mertk
CD4
CD8a
CD62L
Ly108
CD44
CD69
CD27
Ly6G
PD1
Ly6C
F4-80
cKit
NK1-1
Lag3
CX3CR1
Cluster
myeloid/DC
mono/DC
8: monocytes
12: immature mono.
13: CD8- DC
19: CD8a+ DC
24: macrophages
neutrophils
3: immature neut.
4: Il1b+ mature neut.
9: pre-neutrophils
15: G-CSFR^lo neutrophils
16: neutrophil-T cell doublets
18: basophils
22: CCR7+ DC
lymphocytes
17: NK cells
10: B cells
14: plasma cells
23: B1 B cells
T cells
0: naive CD4 T
1: naive CD8 T
2: activated T/Tpex
5: effector CD8
6: in vivo naive/Tcm
7: dividing T
11: Treg
21: dying T cells
20: Tex Myb+ CD8
d0-specific clusters: <10 cells in vitro at d4
d0-specific
E
T cell clusters
myeloid/DC clusters
relative cell count
% of total cells in well
d0 d4
vehicle d4
ruxolitinib d4
F
vehicle
ruxolitinib
MHCII
CD11C
9.13
21.8
%CD11c+ of MHCII+ CD11b-
vehicle_d4
rux_d4
G
Ccl2
Ccl3
Ccl4
Csf2
Il2
Il3
Cluster

Supplementary Figure 2. (**A-G**) B cell-depleted splenocytes from Cl13 infected mice were harvested at 15 days post infection and cultured in the presence of LCMV peptides for 3, 4 or 5 days. (A) Extracellular IFN-γ levels in supernatants of cultures with ruxolitinib or aPD-L1 or vehicle, Bio-plex immunoassay was used to measure IFN-γ. (B) Extracellular cytokine levels 3 and 5 days post stimulation in splenocyte culture in the presence of varying concentrations of ruxolitinib, aPDL1 or vehicle, heatmap shows ratio of cytokine level to vehicle mean. (C) Flow cytometric quantification of intracellular cytokines in T cells at d3 of culture. (D) mRNA marker genes of clusters (left), expression of proteins analyzed by CITE-seq (middle), cluster descriptions (right). Clusters with fewer than 10 cells *in vitro* at d4 of culture are marked as d0-specific clusters. (E) Difference in relative cluster share between d0 and d4 of culture. (F) Splenocytes analyzed by flow cytometry at d4 of culture. (G) Single-cell expression of selected cytokine genes in the in vitro d4 CITE-seq dataset. Experiments were performed once (CITE-seq) or 2-3 times (remaining experiments). Statistical comparison was performed using one-way ANOVA with Dunnett's post-test (A), one-way ANOVA (C), two-tailed Student's t-test (F); Cl13, LCMV clone 13; DC, dendritic cell; *, $p \leq 0.05$; **, $p \leq 0.01$; ***, $p \leq 0.001$; ****, $p \leq 0.0001$.

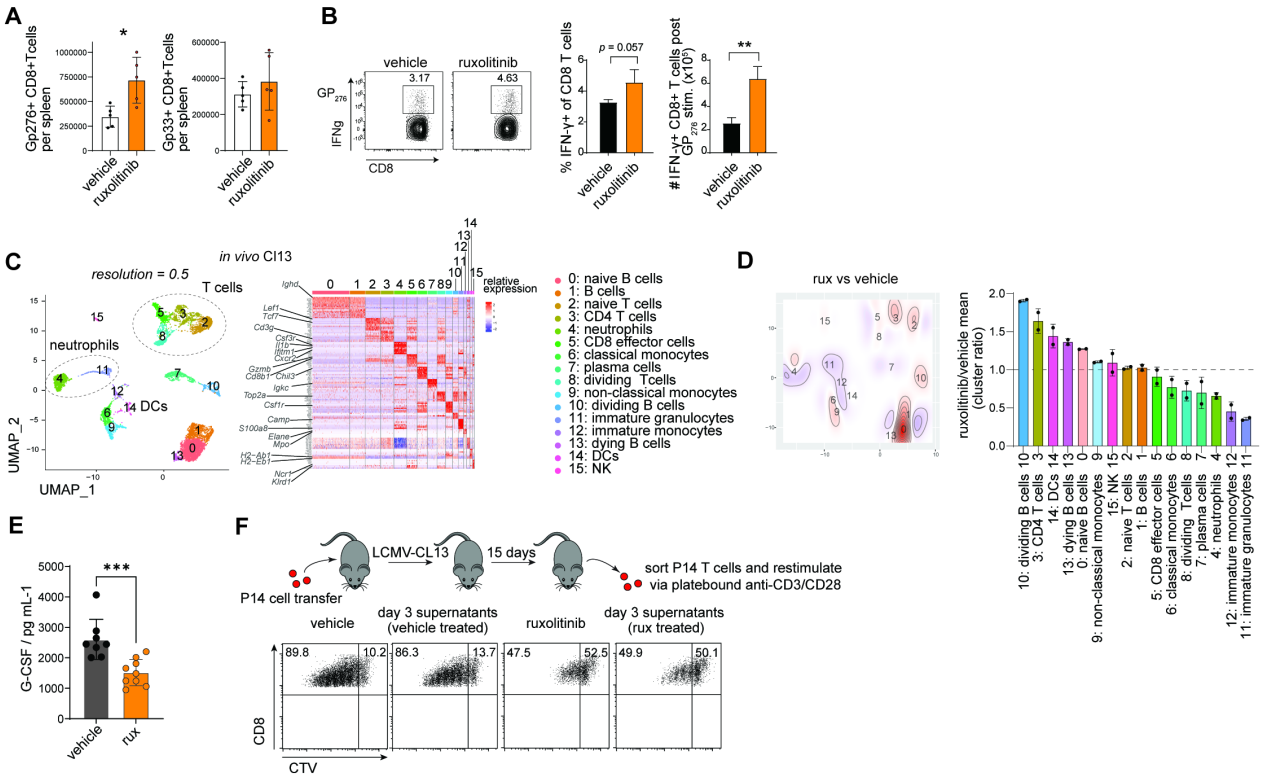

Supplementary Figure 3. Cl13 infected B6 mice were treated with ruxolitinib or vehicle and splenocytes analyzed at 10 dpi: (**A**) total number of virus-specific CD8 T cells per spleen. (**B**) Percentage and number of gp_{276}-stimulated IFNg-producing T cells. (**C**) scRNA-seq analysis of CD45+ splenocytes, dimensionality reduction, clustering and relative cell density in ruxolitinib- vs vehicle-treated mice are shown. (**D**) Relative cell density and cluster ratios of ruxolitinib vs vehicle treated samples. (**E**) Serum cytokine level measured at d5 post infection. (**F**) P14 cells were adoptively transferred to animals infected with Clone 13, then harvested at 15 dpi, stained with CTV dye and stimulated with plate-bound anti-CD3/CD28 in the presence of ruxolitinib or vehicle for 3 days. Experiments were performed once (CITE-seq) or 2-3 times (other experiments). Statistical comparison of experimental groups was performed using Student's two-tailed t-test; Cl13, LCMV Clone 13; *, $p \leq 0.05$; **, $p \leq 0.01$; ***, $p \leq 0.001$.

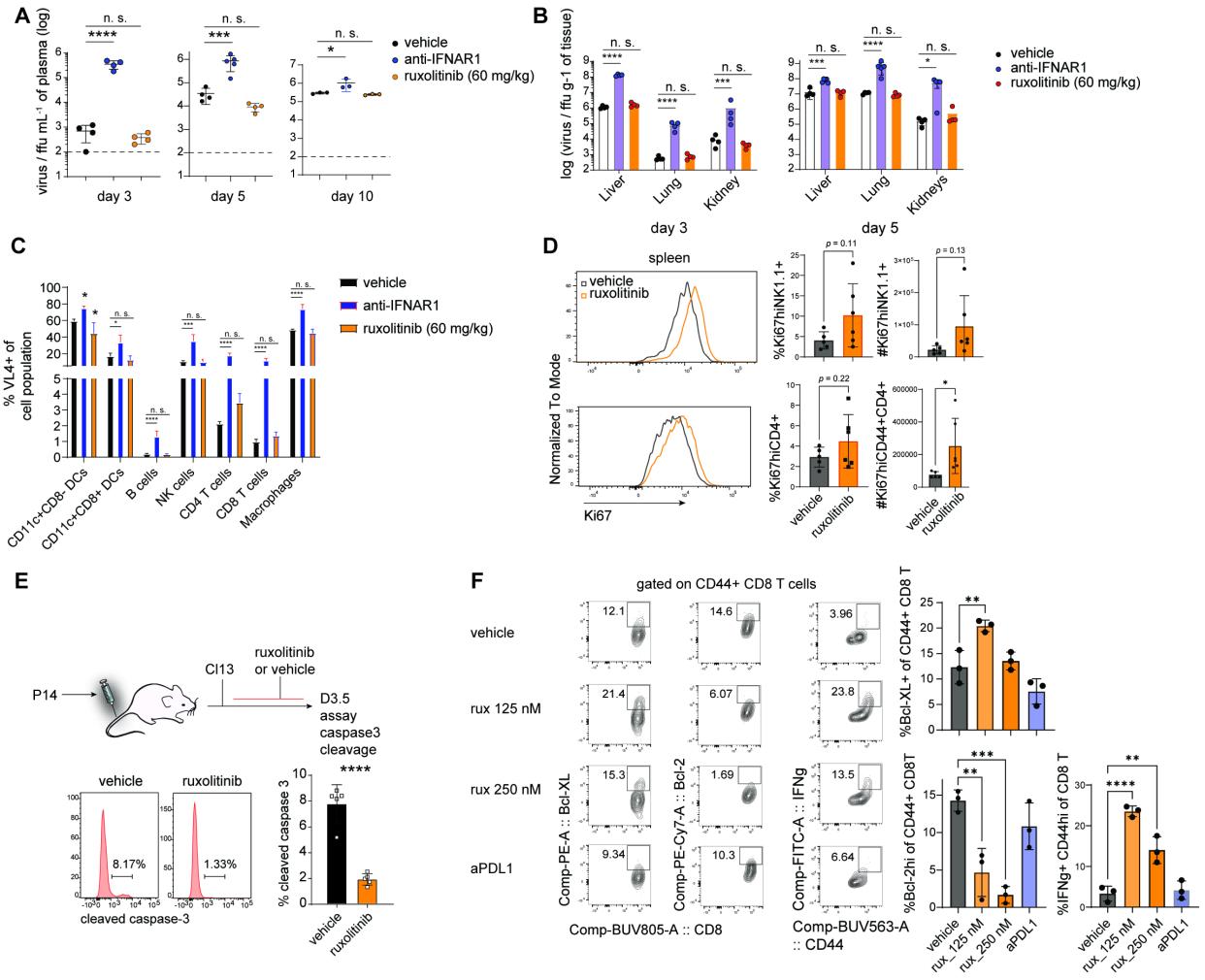

Supplementary Figure 4. (**A-C**) Mice treated with anti-IFNAR1 or isotype 1 day prior to infection with LCMV Cl13 then treated daily with ruxolitinib or vehicle: (A) plasma and (B) tissue LCMV Cl13 titres analyzed at the specified time post infection. (C) Percentage of cells in spleen positive for LCMV protein by cell type. (**D**) Splenic lymphocytes at 10 dpi in Cl13 infected mice treated with ruxolitinib or vehicle. (**E**) Cell death in P14 cells adoptively transferred to Cl13 infected animals treated with ruxolitinib or vehicle and analyzed at 3.5 dpi. (**F**) B cell-depleted splenocytes from Cl13 infected mice were harvested at 15 days post infection and cultured in the presence of LCMV peptides for 5 days then CD8 T cells analyzed by flow cytometry. Statistical comparison of experimental groups was performed using Student's two-tailed t-test (pairwise comparisons) or one-way ANOVA with Dunnett's post-test (A-C) or Sidak's post-test (F); bars show standard deviation. *, $p \leq 0.05$; **, $p \leq 0.01$; ***, $p \leq 0.001$; ****, $p \leq 0.0001$; n. s., not significant.

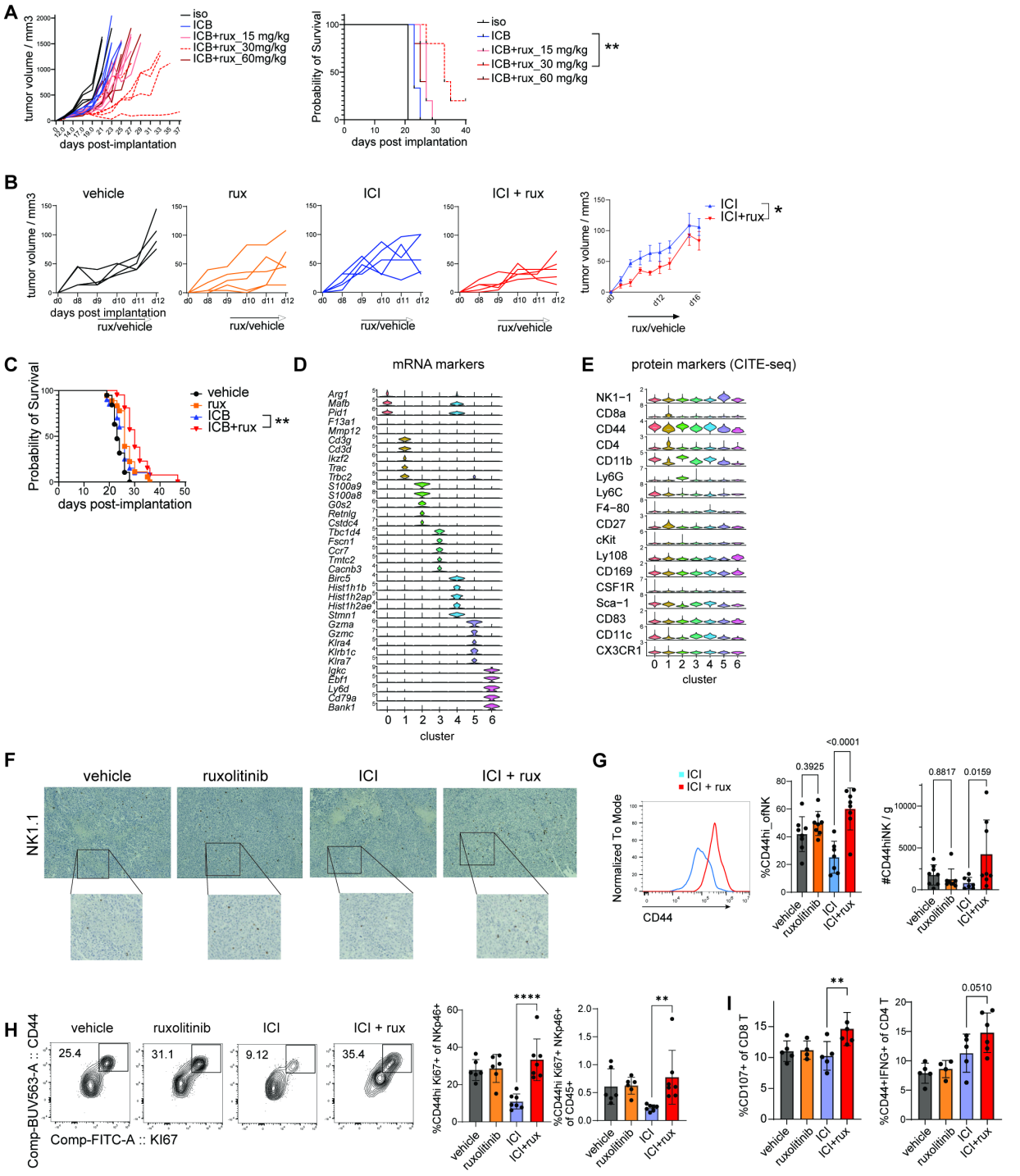

Supplementary Figure 5. (**A**) MC38 tumor bearing mice were treated with ICI and varying concentrations of ruxolitinib (15, 30 or 60 mg/kg or vehicle), tumor size was measured every 2-3 days and survival was defined as reaching a maximum diameter of 15 mm and/or tumor ulceration. (**B-C**) LLC1 tumor bearing mice were treated in four treatment groups equivalent to Fig. 2A and tumor size measured every day. Survival was defined analogously to the MC38 experiment above. (**D-E**) mRNA (D) and protein (E) levels of markers of CITE-seq experiment clusters depicted in Figure 2C. (F-I) MC38 tumor bearing mice treated as in Fig. 2A were

subjected to NK cell analysis by immunohistochemistry (**F**), flow cytometry (**G-H**) and T cell functional analysis by degranulation assay in which cells were incubated with anti-CD107 antibody and PMA/ionomycin for 3h then analyzed by flow cytometry (**I**). Statistical comparison of experiment groups was performed using the log-rank test (A, C), two-way ANOVA (B), one-way ANOVA and Sidak's post-test (G-I); *, $p \leq 0.05$; **, $p \leq 0.01$; ***, $p \leq 0.001$; ****, $p \leq 0.0001$.

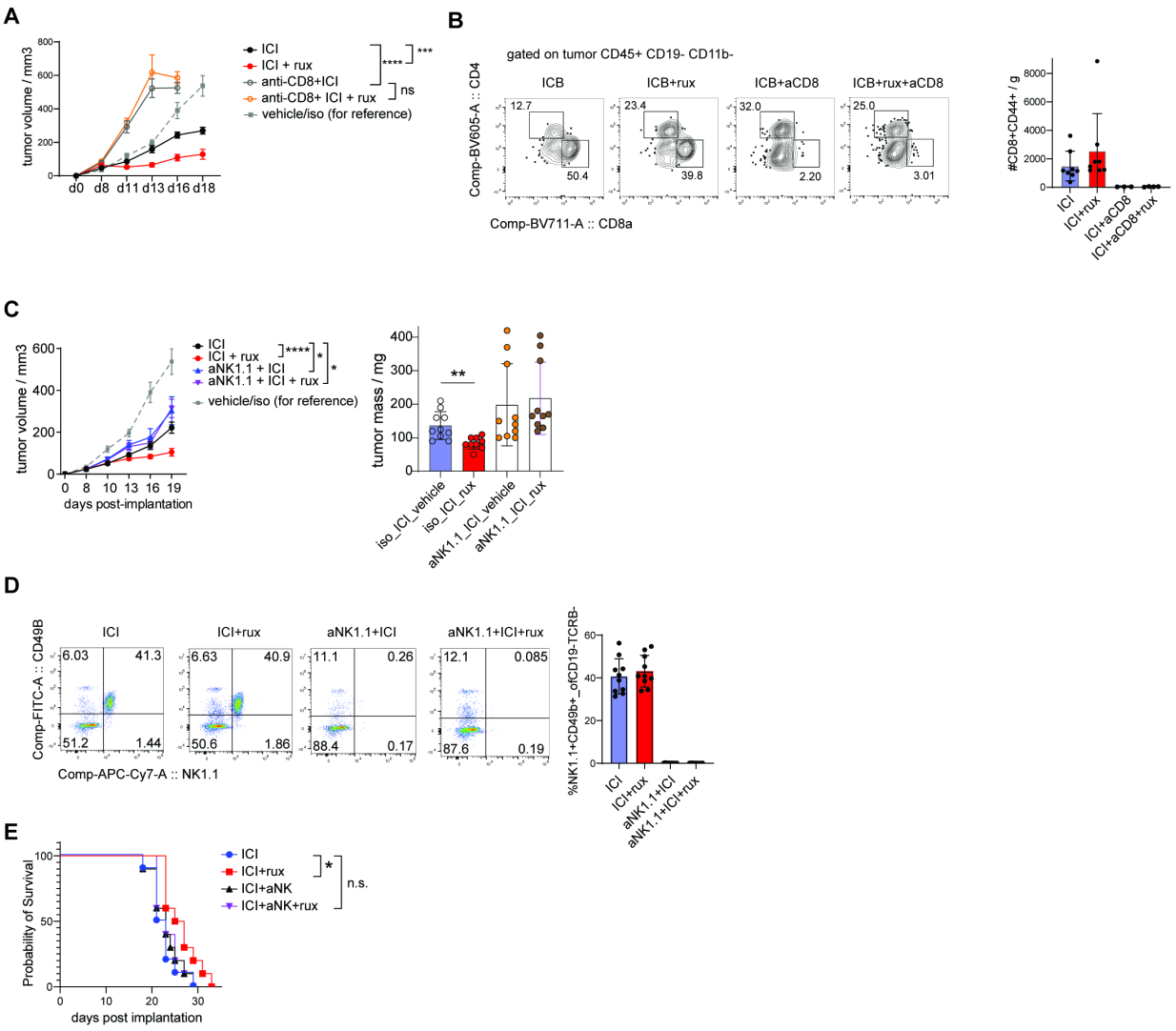

Supplementary Figure 6. (A-B) In MC38 tumor bearing mice treated as described in Fig. 2A, CD8 T cells were depleted using anti-CD8 (Leinco cat #C2442), antibody or respective control antibodies (rat IgG2b) using intraperitoneal injection 1 day before ICI treatment and every 2 days thereafter until end of ICI treatment, tumors were measured every 2-3 days. (B) Tumor-infiltrating CD8 T cells were analyzed by flow cytometry 2 days after second ICI treatment. (**C-E**) MC38 tumor bearing mice were subjected to NK depletion analogous to the CD8 T cell depletion experiment described above. (**D**) Effectivity of NK depletion was assessed by flow cytometry in blood of on-treatment mice. (**E**) Survival curve of mice, survival defined as tumor diameter below 15 mm in any direction or tumor ulceration. Statistical comparison of experimental groups was performed using two-way ANOVA (A, C), one-way ANOVA with Sidak's post-test (C) or the log-rank test (E); *, $p \leq 0.05$; **, $p \leq 0.01$; ***, $p \leq 0.001$; ****, $p \leq 0.0001$.

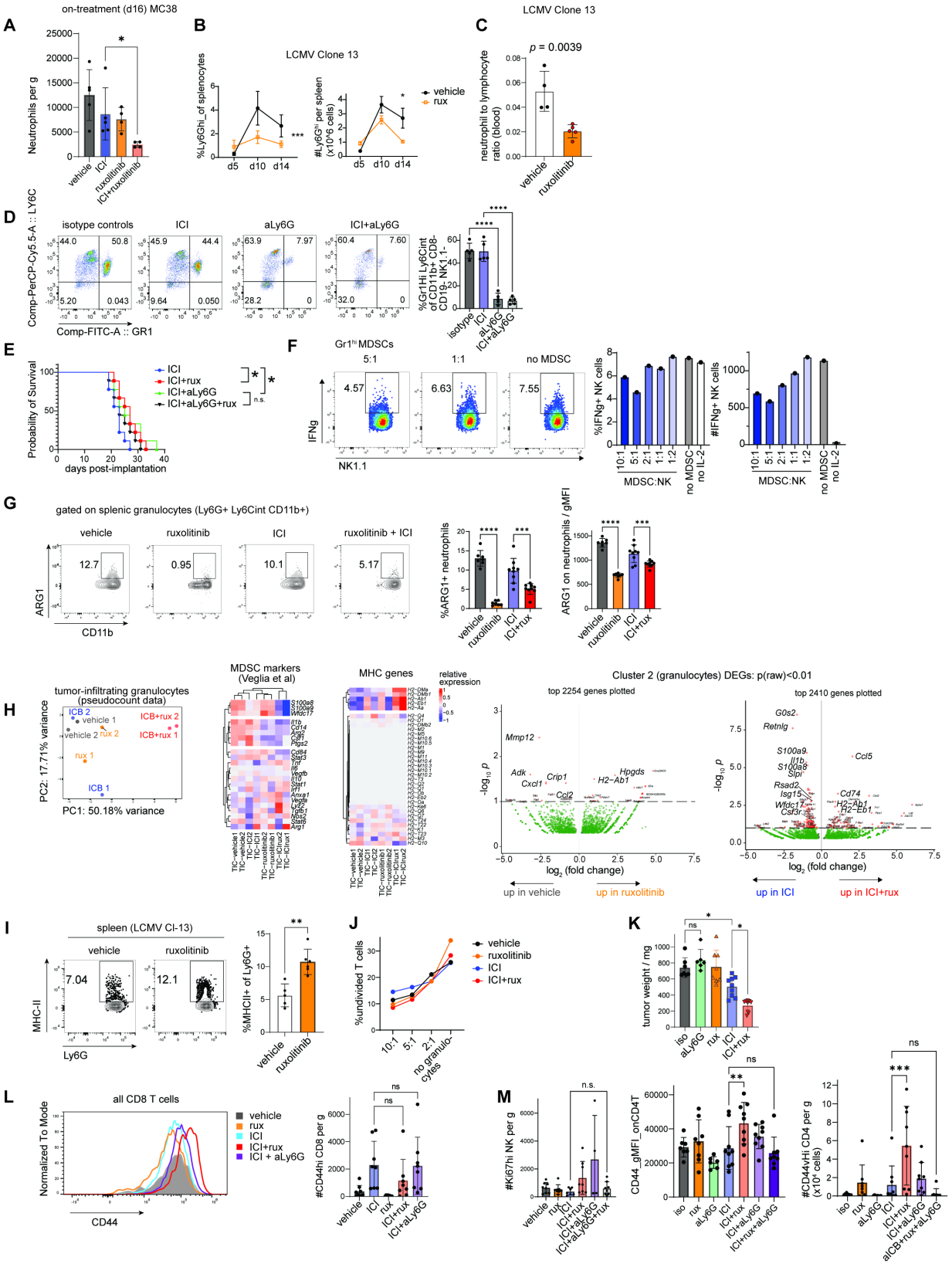

Supplementary Figure 7. (**A**) MC38 tumor bearing mice were treated as described in Fig. 2A. On d16 post implantation, tumor-infiltrating granulocytes were assessed by flow cytometry. (**B-C**) Mice infected with 2x10^6 pfu Cl13 were treated with ruxolitinib or vehicle and granulocytes

examined by flow cytometry on the indicated days post infection. (C) Neutrophil-to-lymphocyte ratio in Cl13 infected mice was calculated as percentage of granulocytes divided by the combined percentage of $CD19^+$ B cells, $CD3^+$ T cells and $NK1.1^+$ NK cells of CD45+ peripheral blood cells. (**D-E**) MC38 tumor bearing mice were treated with Ly6G-depleting antibody or isotype control 2 days prior to treatment with ICI/isotype and ruxolitinib/vehicle, then every 2 days until end of ruxolitinib/vehicle treatment, tumor volume measured every 2-4 days. (D) Blood granulocytes were analyzed using Gr1 antibody to verify the effectivity of granulocyte depletion on day 12 post implantation (1 day after 2^{nd} anti-Gr1 dose). (E) Survival curve of mice in the granulocyte depletion experiment. (**F**) Tumor-infiltrating myeloid derived suppressor cells from MC38 tumor bearing mice were isolated and subjected to NK cell suppression assay (*76*). (**G**) MC38 tumor bearing mice were treated as in Figure 2A, splenic granulocytes analyzed 2 days after treatment cessation. (**H**) Principal component analysis, relative expression of selected genes and volcano plot depicting differential expression analysis of RNA-seq dataset described in Figure 3B. (**I**) Splenic granulocytes from Cl13 infected mice treated with ruxolitinib or vehicle at 10 dpi. (**J**) Percentage of undivided cells of all live cells in T cell stimulation assay described in Figure 3D. (**K**) MC38 tumor bearing mice were treated as in Figure 2A with the additional experiment group treated with anti-Ly6G two days prior to treatment with isotype and vehicle, then every 2 days until end of vehicle treatment. (**L**) Tumor-infiltrating cells in mice treated as in Figure 3C were analyzed 2 days post treatment. (**M**) Tumor-infiltrating cells in mice treated as described in Figure 3E were analyzed 2 days post treatment. Experiments were performed once (RNA-seq) or 2-3 times (other experiments); representative results shown for repeated experiments. Statistical comparison of experimental groups was performed using one-way ANOVA with Sidak's post-test (A, D, G, K, L), two-way ANOVA (B), log-rank test (E), DESeq2 Wald test (H).

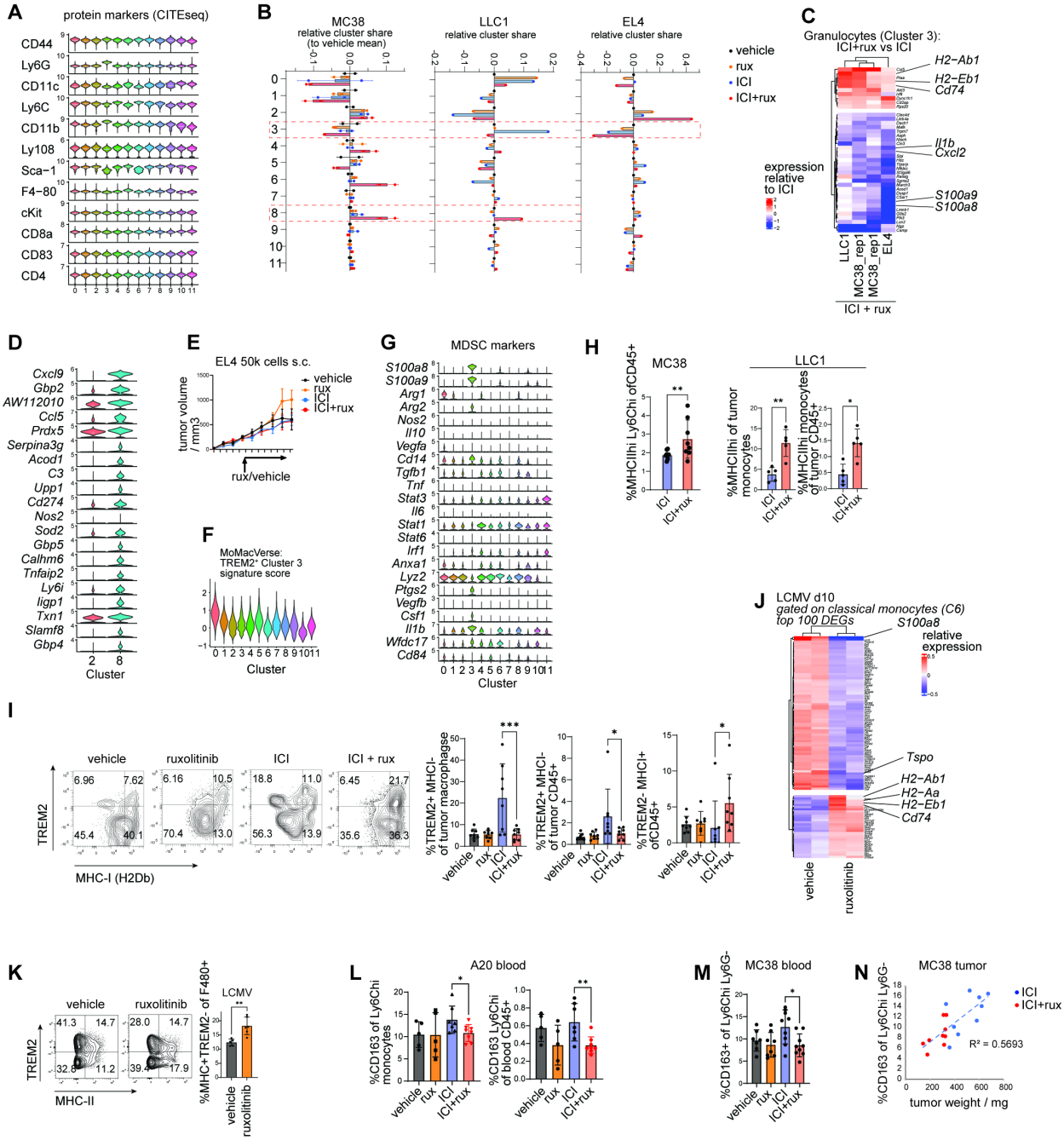

Supplementary Figure 8. (**A-D, F-G**) Myeloid cells from tumor bearing mice were analyzed by CITE-seq and data integrated. (A) Protein markers of CITE-seq dataset in Figure 4A. (B) Relative cluster share of cells in each sample calculated using the following formula: fraction of sample cells in cluster – average fraction of cells in cluster in vehicle treated controls. Vehicle treated controls specific to each tumor types were used. (C) Differential expression analysis in ICI+rux vs ICI treated mice, gated on tumor-infiltrating granulocytes. Heatmap shows relative expression of differentially expressed genes in ICI+rux vs ICI treated mice based on pseudobulk expression values. (D) Genes differentially expressed between Clusters 2 and 8 of the integrated CITE-seq dataset. (**E**) Tumor growth of EL4 tumors in mice treated with vehicle, ruxolitinib, ICI or ICI+rux analogous to MC38 experiments. (F) relative expression of MoMac-VERSE Cluster 3

signature in myeloid clusters described in Figure 4A. (G) Relative expression of MDSC markers in CITE-seq clusters described in Figure 4A. (**H**) Tumor-infiltrating monocytic cells from mice bearing MC38 or LLC1 tumors and treated as in Figure 2A were analyzed by flow cytometry 2 days after cessation of treatment. (**I**) Tumor-infiltrating macrophages in mice treated as in Fig. 2A were analyzed by flow cytometry 2 days after treatment. (**J**) Top differentially expressed genes in splenic classical monocytes in ruxolitinib vs vehicle treated Clone 13 infected mice 10 dpi, gated on Cluster 6 from Figure S3C. (**K**) Flow cytometry analysis gated on splenic macrophages (F4/80+ Ly6G- CD11b-) in Clone 13 infected mice 10 dpi. (**L**) A20 tumor bearing mice were treated with vehicle, ruxolitinib, ICI or ICI + ruxolitinib analogous to Figure 2B and blood cells analyzed by flow cytometry on day 25 post implantation. (**M-N**) Tumor-infiltrating monocytic cells from mice bearing MC38 tumors and treated as in Figure 2A were analyzed by flow cytometry and weighed 2 days after cessation of treatment. Experiments were performed once (CITE-seq) or 2-4 times (other experiments). Statistical comparison of experimental groups was performed using the DESeq2 Wald test (C, J), Wilcoxon rank sum test (D), two-tailed Student's t-test (H, K), one-way ANOVA with Sidak's post test (I, L-M) and the Coefficient of determination (N). *, $p \leq 0.05$; **, $p \leq 0.01$; ***, $p \leq 0.001$; ****, $p \leq 0.0001$.

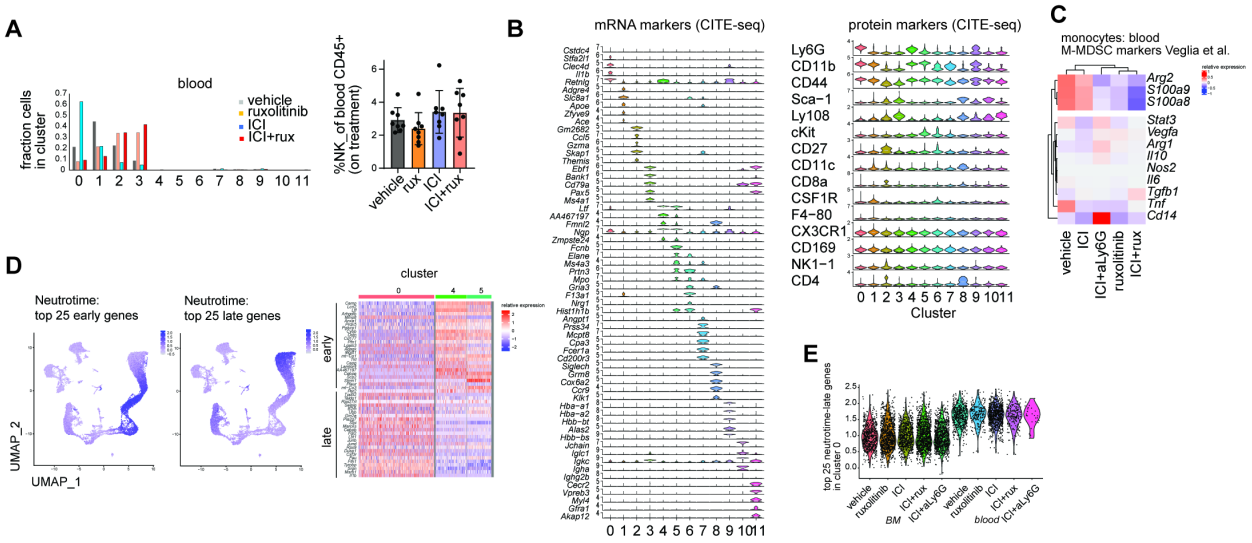

Supplementary Figure 9. (**A-E**) Bone marrow and blood from mice treated as in Fig. 2A were analyzed by CITE-seq and flow cytometry in independent experiments. (A) Absolute fraction of cells in sample per cluster divided by treatment group (left); flow cytometric analysis of NK cells in blood in the respective treatment groups (right). (B) Relative expression of mRNA (left) and protein (right) markers. (C) Relative expression of M-MDSC markers in blood monocytes (Cluster 1 from CITE-seq dataset described in Figure 4D). (D) Relative expression of early and late neutrophil differentiation signatures in CITE-seq dataset in Figure 4D, top 25 early and late Neutrotime genes were selected for analysis**.** (E) Relative expression of gene signature comprising top 25 late Neutrotime genes in Cluster 0 of CITE-seq dataset in Figure 4D. Experiments were performed once (CITE-seq) or 2-3 times (flow cytometry), representative flow cytometry data shown. Statistical analysis of CITE-seq data was performed using Seurat v4.

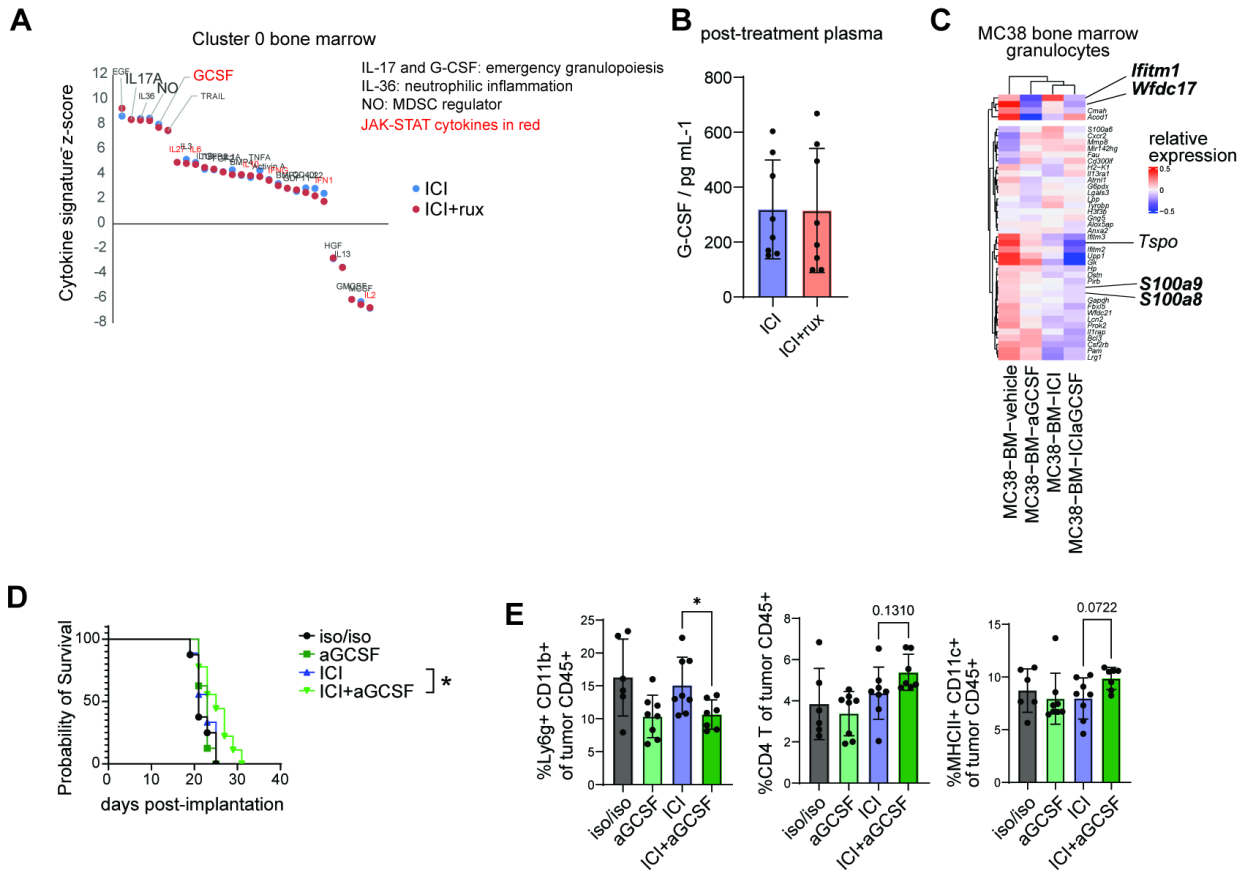

Supplementary Figure 10. (**A**) Cytokine transcriptomic signature scores in bone marrow cells in Cluster 0 defined in Figure 4D, cytokine signatures quantified by CytoSig (*38*), important myeloid and MDSC cytokines highlighted. (**B**) Plasma G-CSF levels in MC38 tumor bearing mice treated as in Figure 2A and analyzed 2 days post treatment. (C-E) MC38 tumor bearing mice were treated with low-dose G-CSF neutralizing antibody or isotype control every 3 days once palpable and ICI or isotype control once palpable and 7 days later, bone marrow granulocytes analyzed by CITE-seq 2 days after end of treatment. (**C**) Heatmap shows relative expression of ruxolitinib-downregulated genes. (**D**) Survival analysis of mice defined as tumor size below 15 mm in all diameters and free of ulceration. (**E**) Flow cytometry of tumor-infiltrating cells collected 2 days after 2nd ICI injection. Experiments were performed once (CITE-seq) or 2-3 times (all other experiments) for which representative results are shown. Statistical comparison of experimental groups was performed using DESeq2 (C), log-rank test (D) and one-way ANOVA with Sidak's post test (E). *, $p < 0.05$.

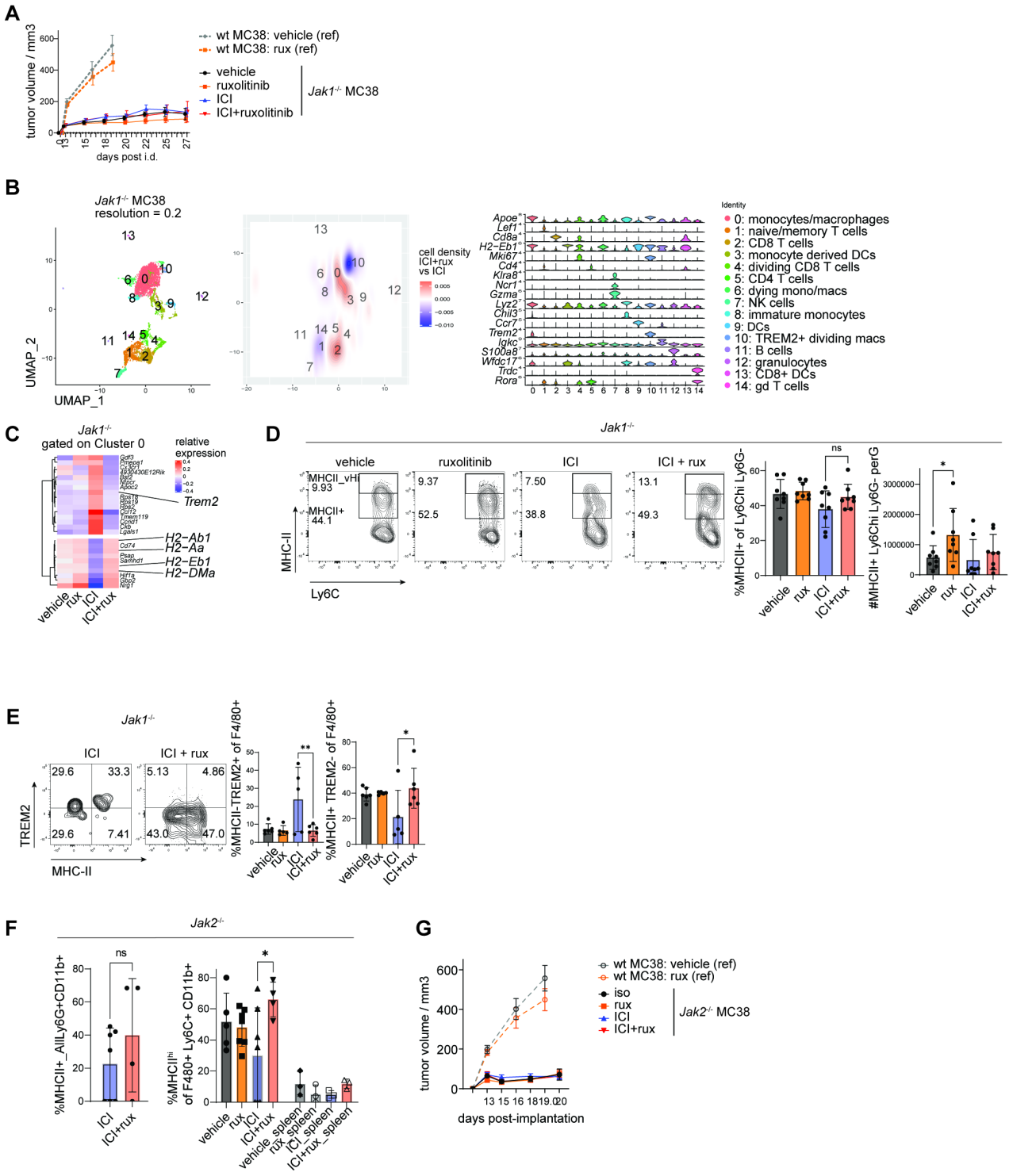

Supplementary Figure 11. Mice bearing *Jak1*$^{-/-}$ (**A-E**) or *Jak2*$^{-/-}$ (**F-G**) MC38 tumors were treated with ICI and ruxolitinib or vehicle analogous to Fig. 2A, treatment starting when tumors were palpable and tumor-infiltrating granulocytes analyzed 2 days post treatment**.** (A) Tumor volumes of *Jak1*$^{-/-}$ MC38 tumors; reference values for wt MC38 tumors in an equivalent experiment treated with vehicle or ruxolitinib are shown. (B) Single-cell transcriptomic analysis of tumor-infiltrating CD45^{+} cells: dimensionality reduction and clustering (left), relative density

of cells in ICI+rux vs ICI treated tumors (middle); relative expression of selected mRNA cluster markers (right). (C) Genes differentially expressed between ICI+rux and ICI treated groups in Cluster 0. (D) Flow cytometry of tumor-infiltrating monocytes ($Ly6C^{hi}$ $CD11b^{+}$ $Ly6G^{-}$). (E) Flow cytometry analysis of tumor macrophages. (F) Flow cytometry studies in *Jak2*$^{-/-}$ MC38 tumors, gated on granulocytes (left) and macrophages (right). (G) Tumor volumes of *Jak2*$^{-/-}$ MC38 tumors; reference values for wt MC38 tumors in an equivalent experiment treated with vehicle or ruxolitinib are shown. Experiments were performed once (scRNAseq) or 2-3 times (all other experiments); representative results are shown for the latter. Statistical comparison of experimental groups was performed using DESeq2 (C) or one-way ANOVA with Sidak's post test (D-F); *, $p < 0.05$; **, $p \leq 0.01$.

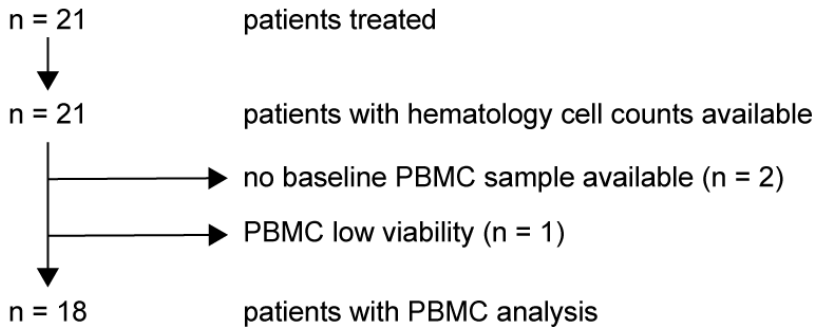

Supplementary Figure 12. Details on the number of patients with complete blood cell counts data and PBMC samples available. PBMC, peripheral blood mononuclear cell.

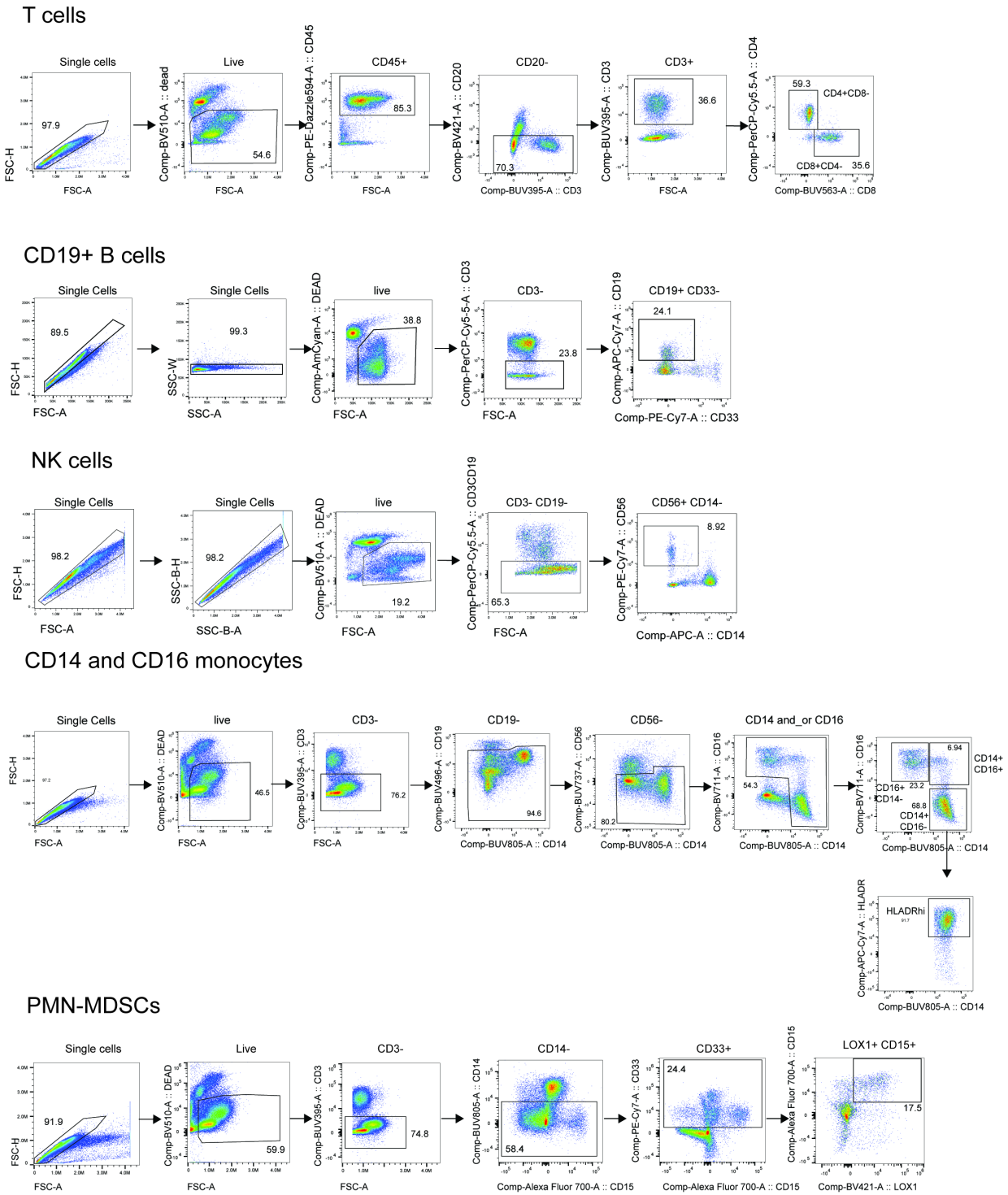

Supplementary Figure 13. Gating strategies for major blood cell populations analyzed in patient PBMCs.

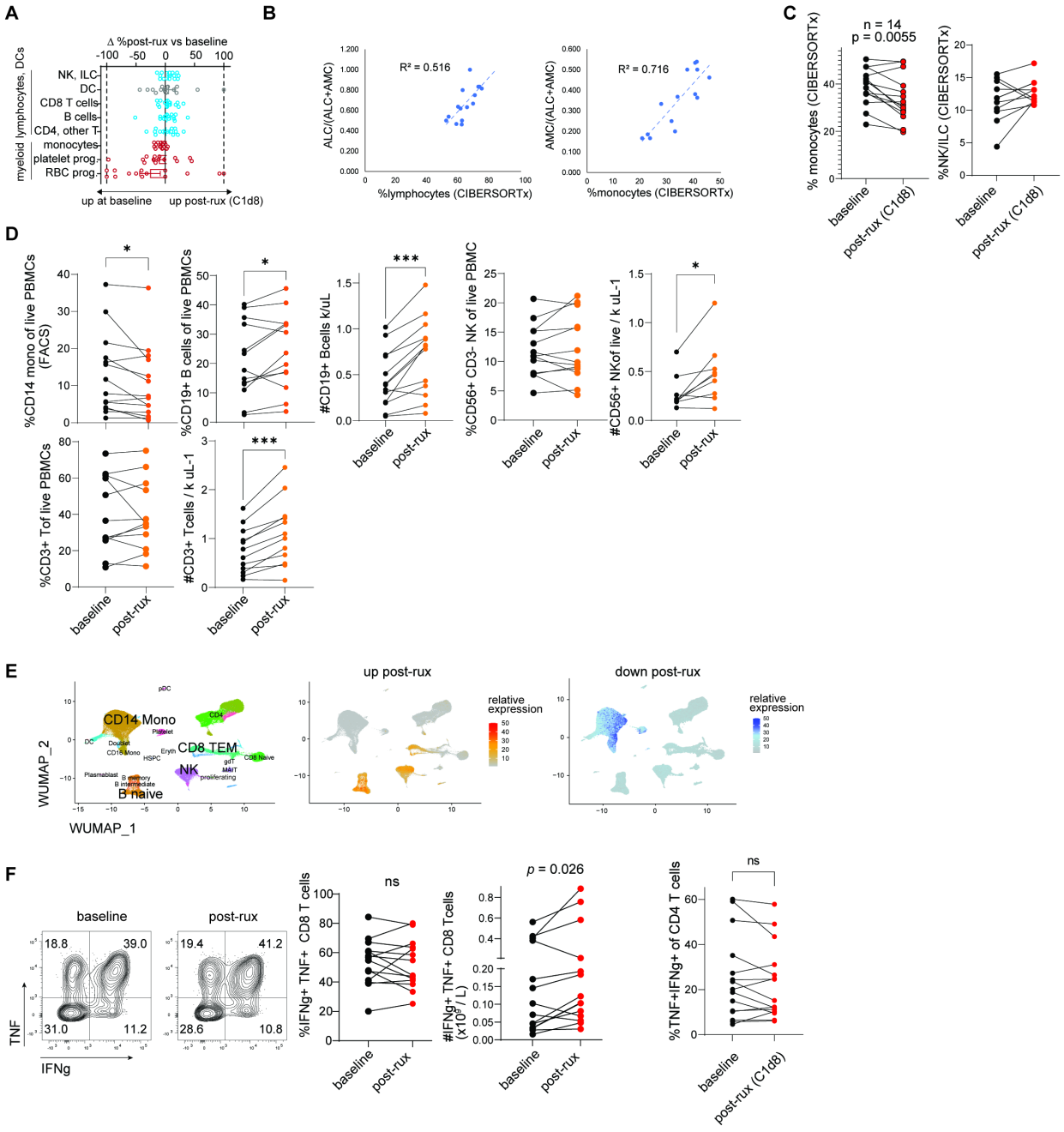

Supplementary Figure 14. (**A**) Peripheral blood cells examined by bulk RNA-sequencing (RNA-seq) and cell type percentages estimated using CIBERSORTx with custom single-cell RNA-seq reference data. (**B**) Comparison of absolute lymphocyte count (ALC) as fraction of absolute monocyte count and ALC combined vs CIBERSORTx-predicted percentage of lymphocyte (left), AMC as fraction of AMC and ALC combined vs predicted monocyte fraction in PBMC (right). (**C**) Change in predicted monocyte and NK/ILC percentage after ruxolitinib vs baseline. (**D**) Changes in major cell types post-ruxolitinib vs baseline, assessed by flow cytometry. Flow cytometry and absolute lymphocyte counts were used to estimate the changes in absolute concentration of the cell types in peripheral blood. (**E**) Expression pattern of ruxolitinib-upregulated and -downregulated genes in a dataset of normal donor PBMCs (*87*); (**F**) Percentage

of cytokine-producing T cells of CD8 and CD4 T cells in patient PBMCs in a PMA/ionomycin stimulation assay. Statistical comparison of post-ruxolitinib and baseline samples was performed using two-tailed Student's ratio paired test (C-D, F). Correlation analysis was performed using the Coefficient of determination (B). *, $p < 0.05$; **, $p \leq 0.01$; ***, $p \leq 0.001$.

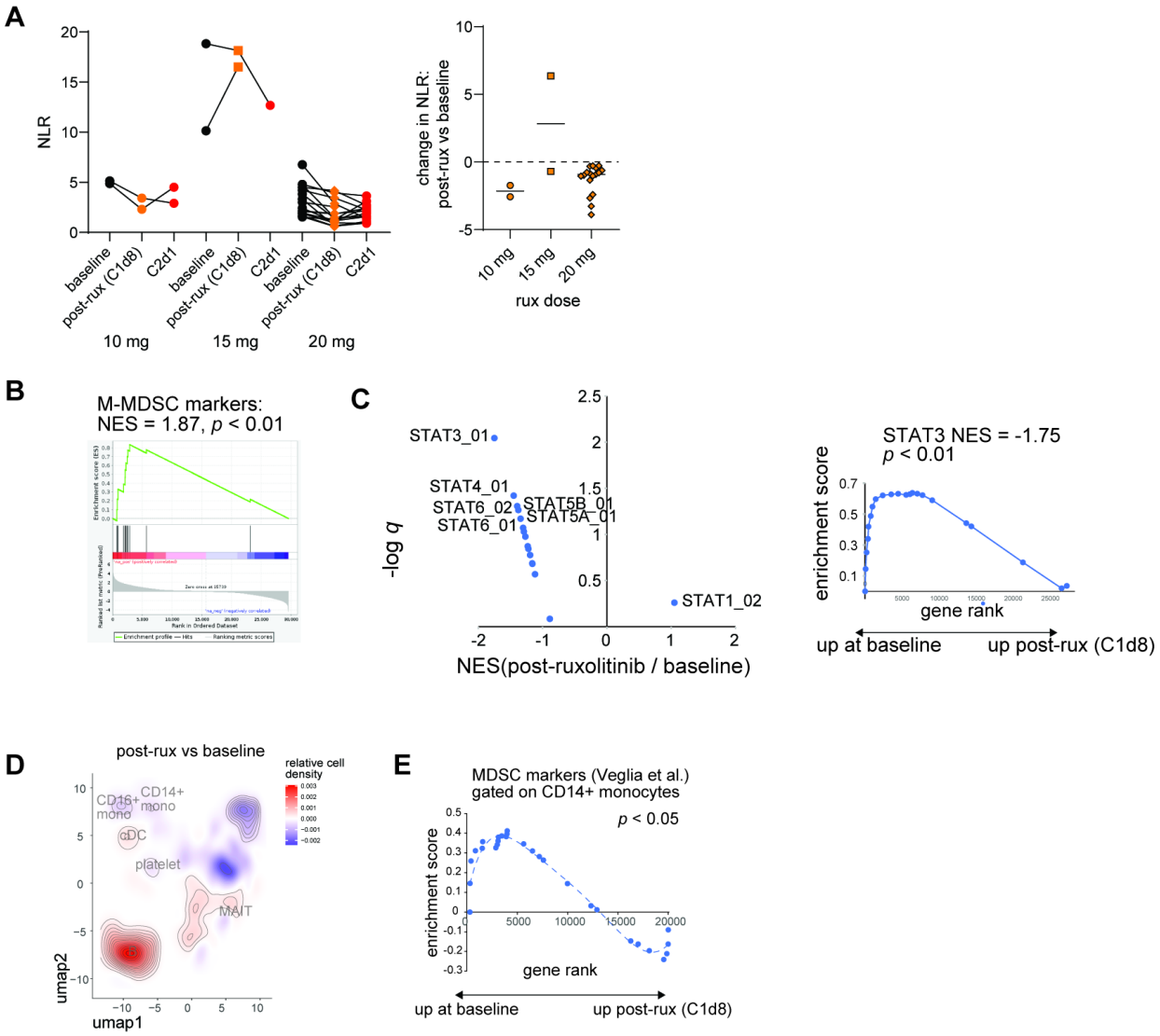

Supplementary Figure 15. (**A**) Neutrophil-to-lymphocyte ratio in patients grouped by ruxolitinib dose. (**B**) GSEA of M-MDSC and PMN-MDSC genesets from Veglia et al. calculated using bulk RNA-seq data. (**C**) Normalized enrichment scores from GSEA analysis and q values of STAT gene sets in PBMC bulk-seq data. (**D**) Relative density of post-ruxolitinib vs baseline single cells on dimensionality reduced embedding. Density change was calculated using data described in Figure 5H. (**E**) MDSC signature score expression before and after ruxolitinib specifically in $CD14^{+}$ monocytes, GSEA plot shows change in combined MDSC marker geneset. Statistical comparison of post-ruxolitinib and baseline timepoints was performed using paired GSEA. GSEA, gene set enrichment analysis.

A

Dose level (bid)	Number of patients treated	Number of evaluable patients	Best response (2023)
10 mg	2	2	PR, PD
15 mg	2	1	PR
20 mg	17	16	6xCR, 1xIR2, 1xPR, 2xSD, 6xPD

B

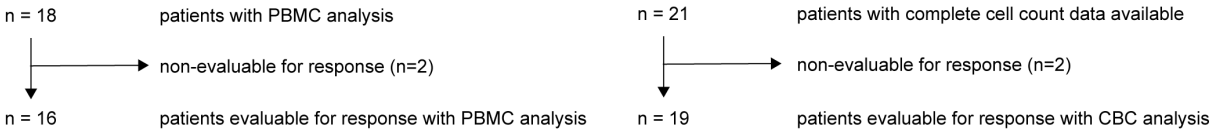

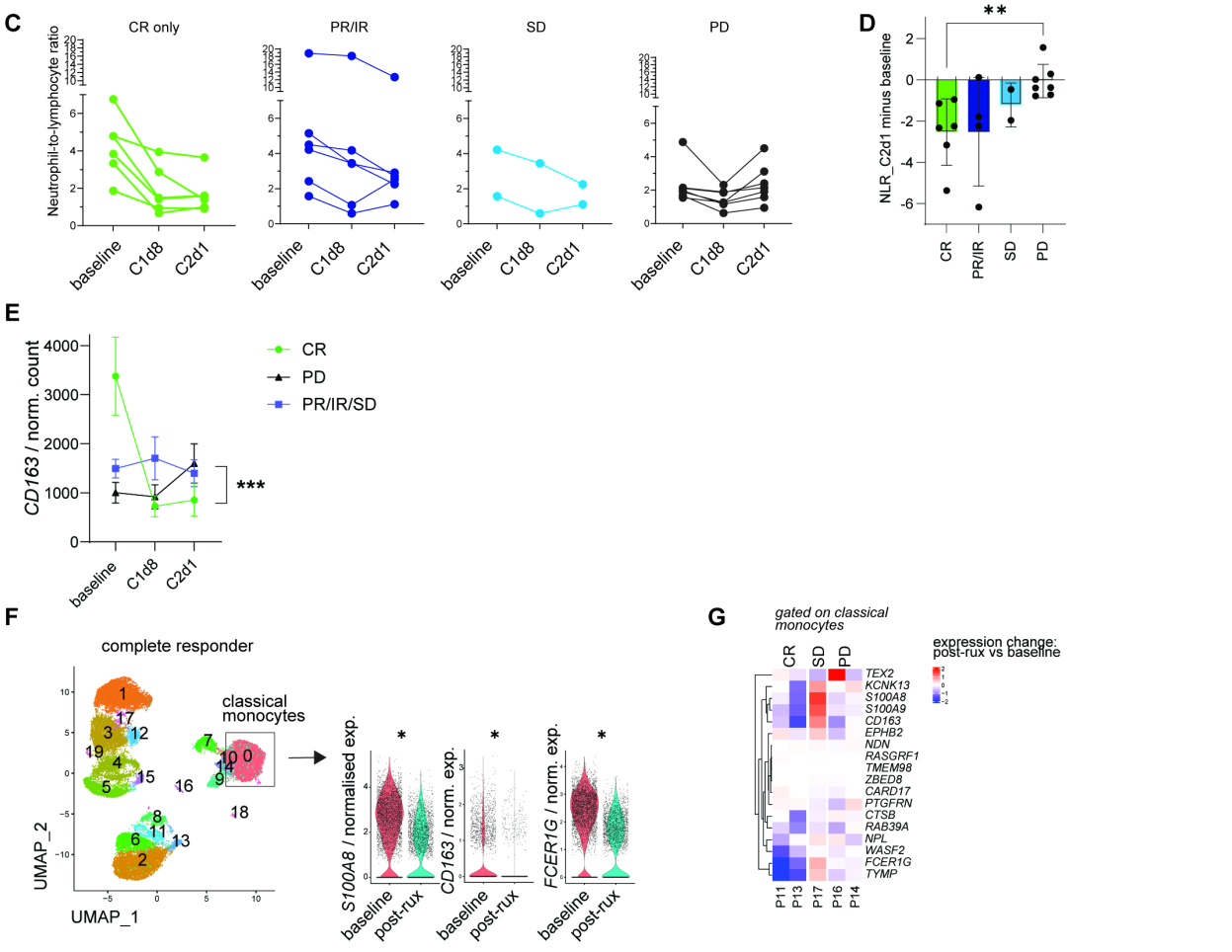

Supplementary Figure 16. (**A**) Details on the number of patients treated with each dose of ruxolitinib and their best clinical response. (**B**) Details on the number of patients evaluable for response for whom PBMC and CBC analysis were performed. (**C**) Changes in the neutrophil-to-lymphocyte ratio in patients grouped by best response category. (**D**) The change in the neutrophil-to-lymphocyte ratio post-nivolumab with ruxolitinib (Cycle 2, day 1) vs baseline in patients grouped by best response. (**E**) Normalized expression of *CD163* in PBMCs during

treatment in patients grouped by best response category. (**F**) Single-cell transcriptome analysis of PBMCs from an example complete responder, gene expression changes gated on cluster 0 (classical monocytes). (**G**) Relative gene expression post-ruxolitinib vs baseline in classical monocytes in 5 patients, based on scRNA-seq data. CR, complete response; PR, partial response; IR, indeterminate response; SD, stable disease; PD, progressive disease; NLR, neutrophil-to-lymphocyte ratio. Statistical analysis was performed using two-tailed Student's t-test (D), two-way ANOVA (E) and Wilcoxon rank sum test (F); *, $p < 0.05$; **, $p \leq 0.01$; ***, $p \leq 0.001$.

Granulocytes and monocytes

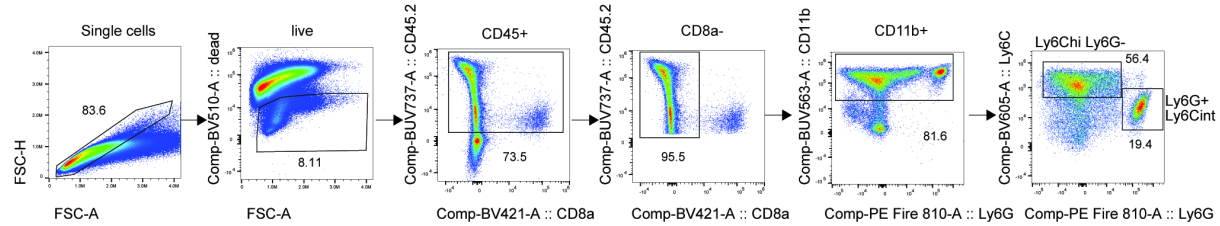

CD11b+ dendritic cells e.g. in Fig. 1D

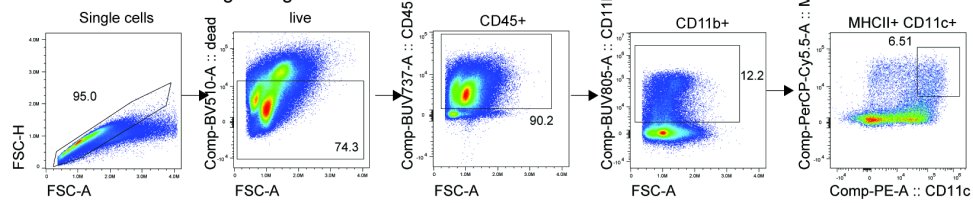

Tumor macrophages

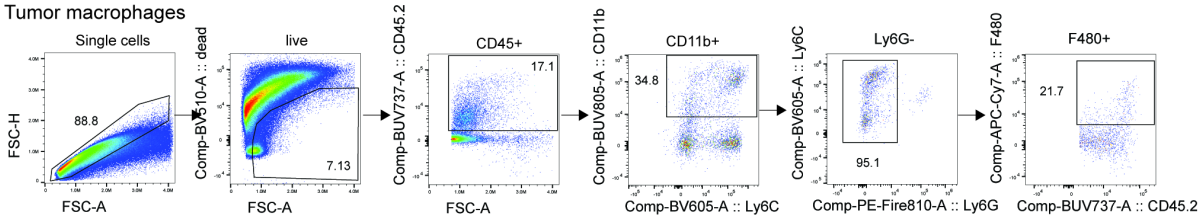

CD4 and CD8 T cells

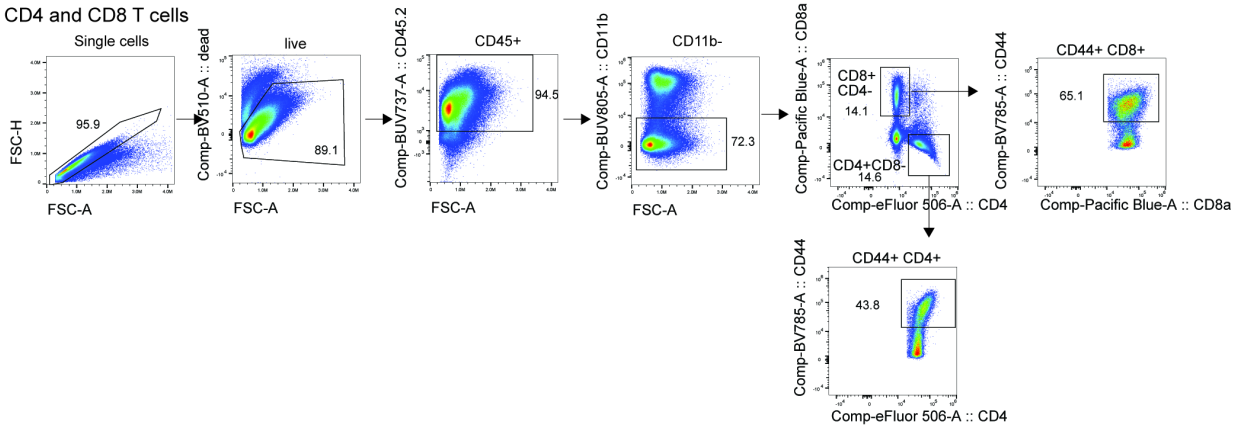

NK cells

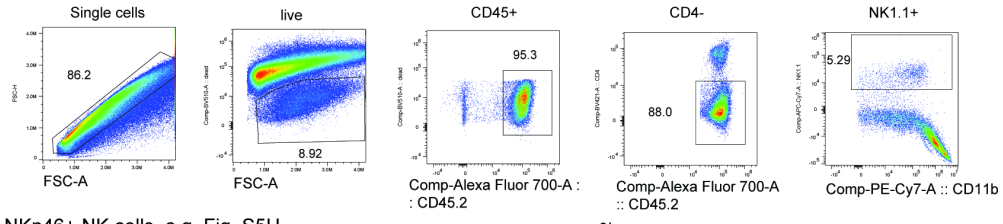

NKp46+ NK cells, e.g. Fig. S5H

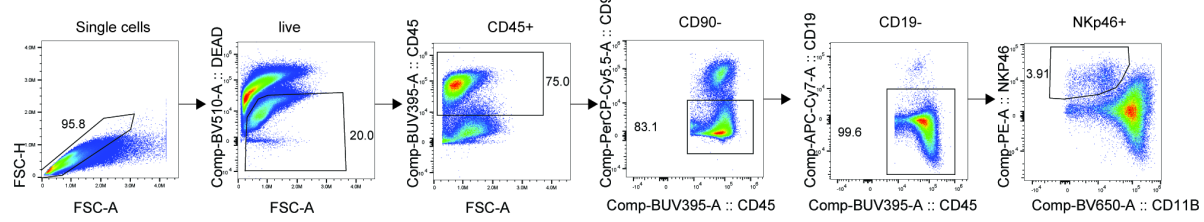

Supplementary Figure 17. Gating strategies for mouse cell populations analyzed in this study.

Supplementary Table 1. Patients, disease and treatment characteristics. ICI, immune checkpoint inhibitor.

Variable	All patients (n=19)
Age (in years; median; range)	38 (22-76)
Gender: Male n (%)	13 (68%)
Race: White n (%)	17 (89%)
Time from diagnosis to enrollment Median (range in years)	3.4 (0.9-16.7)
Stage at Diagnosis n (%) II III-IV	 2 (11%) 17 (88%)
Prior lines of therapy: Median (range)	4 (2-11)
Prior hematopoietic cell transplantation: Autologous Allogeneic Both auto and allogeneic	13 (68%) 8 (42%) 2 (11%) 3 (16%)
Prior Pembrolizumab Prior Nivolumab	9 (47%) 10 (53%)
Refractory to ICI (progressed while on ICI)	11 (58%)
Duration of remission on prior ICI Median (range in months)	 5.1 (0.9-46.3)
Time from past ICI to enrollment Median (range, in months)	 11.7 (2.0-48.1)

Supplementary Table 2. Adverse events definitely or probably related to combination of nivolumab with ruxolitinib. AEs were graded using CTCAE v5.0.

Variable	Count
Median number of cycles	8 (range 3-24 cycles)
DLT events	0
Nausea grades 1,2	3,2
Anemia grade 2,3	1,1
Neutropenia grade 1	1
Infections – pneumonia grade 3	1
Herpes zoster grade 2	1
Auto-immune toxicities – total	5
Pulmonary grade 3	1
LFTs abnormalities grade 1, 2	1, 2
Autoimmune hepatitis grade 3	1
Arthralgias grade 1	1
Elevated TSH grade 2	1

5

Supplementary Table 3. Details on patient subgroups subjected to specific cellular and molecular analyses.

Patient number	Evaluable for response (Fig. 5B)	ALC (Fig. 5C)	NLR (Fig. 5D)	bulk RNA-seq (Fig. 5E, 5G, 5K)	PMN-MDSC FACS (Fig. 5F)	single-cell RNAseq (Fig. 5H)
1	+	+	+	+	+	
2	+	+	+	+		
3		+	+	+	+	
4	+	+	+	+		
5	+	+	+		+	
6	+	+	+	+	+	
7	+	+	+	+		
8	+	+	+			
9		+	+	+		
10	+	+	+	+		
11	+	+	+	+		+
12	+	+	+		+	
13	+	+	+	+	+	+
14	+	+	+	+		+
15	+	+	+	+	+	
16	+	+	+	+		+
17	+	+	+	+	+	+
18	+	+	+	+	+	
19	+	+	+	+	+	
20	+	+	+	+	+	
21	+	+	+	+	+	
Total count	19	21	21	18	12	5